

A study of the electronic and ionic structure, for competing states of fully and partially ionized hydrogen, using the neutral pseudo-atom method as well as a classical map for the electron subsystem.

M.W.C. Dharma-wardana^{1,2,*}

¹*Département de Physique, Université de Montréal, Montréal, Québec, Canada H3C 3J7*

²*National Research Council of Canada, Ottawa, Ontario. Canada K1A 0R6*

Prof. Bonitz and his collaborators have made seminal contributions to the study of the uniform electron fluid and the electron-proton fluid, viz., hydrogen, in using *ab initio* simulations. as reflected in this festschrift. Here we review the theoretical methods available for these systems where traditional small-parameter methods fail. We use the neutral-pseudo atom (NPA) method, and a classical map for quantum electrons to study hydrogen plasmas. We show that *both* fully-ionized and partially-ionized hydrogen phases can exist with the same nominal density and temperature, at pressures and temperatures of interest to planetary physics. The mean ionization \bar{Z} , pair-distribution functions, free energies, pressures and conductivities are calculated for the competing phases. Here \bar{Z} is also a measure of the miscibility of fully ionized and un-ionized hydrogen. Recent studies using path-integral Monte Carlo methods, and N -atom Density Functional Theory (DFT) simulations have provided essential structure data including the electron-electron structure factor $S_{ee}(k)$ that enters into interpretation of X-ray Thomson scattering and other diagnostics. We show that these structure data can be inexpensively evaluated using classical-map schemes for fully ionized plasmas, and more generally, using one-atom (average-atom) DFT methods for partially ionized systems.

PACS numbers: 52.25.Jm,52.70.La,71.15.Mb,52.27.Gr

Conflict of Interest - The author declares no conflict of interest related to this research.

Funding - This research did not receive any specific grant or funding from any sources in the public, commercial, or not-for-profit sectors.

Data availability - All data used in the paper are available within the paper graphically or otherwise, and also by reasonable request from the author.

ORCID 0000-0001-8987-9071

I. INTRODUCTION

The advent of high-energy lasers and femto- and even atto-second technologies [1] have made it possible to create and study matter under extreme conditions [2, 3]. Prof. Michael Bonitz and his collaborators have made seminal contributions to the *ab initio* study of such systems [4–6], as reflected in this Festschrift.

Material systems under extreme densities $\bar{\rho}$, and temperatures T , with extreme pressures P occur naturally in planetary interiors and astrophysical objects. They also occur as transient states that have to be probed on sub-nanosecond timescales [3, 7–11]. These involve cutting-edge experiments on high-energy-density materials relevant to experimental astrophysics [8], fusion

physics [9, 10] and even for nuclear-stockpile stewardship requirements. The Fermi energies E_F of compressed matter are large, and although T (where we use energy units) may be nominally high, $\theta = T/E_F$ is of the order of unity. Hence the name “warm-dense matter” (WDM) has been used for such highly-correlated energy-dense matter.

The number of free-electrons per ion, viz., \bar{Z} , the interaction potentials, static structure factors $S_{ab}(k)$ where $a, b = e, i$ (i.e., electrons, ions) as well as their dynamic analogues, e.g., $S_{ab}(k, \omega)$ [12] are relevant to the evaluation of the equation of state [10, 13], and transport properties [13, 14] of WDM. They appear in the analysis of experimental results from X-ray Thomson scattering (XRTS) [15–19] and X-ray diffraction [7, 11, 20, 21]. The theoretical methods available for the study of WDM hydrogen and the uniform electron fluid (UEF) include the following.

1. N -atom density-functional calculations, coupled with molecular dynamics (DFT-MD) where N nuclei and the corresponding number of electrons are treated using Kohn-Sham-Mermin density functional theory (DFT). Here the ion configurations are evolved using classical molecular dynamics (MD). This method is referred to as DFT-MD, or more frequently as QMD (quantum MD).
2. Path-Integral-Monte-Carlo (PIMC) methods. Here the partition function is evaluated using Feynman trajectories, and works most efficiently at high- T where the trajectories are close to classical trajectories.
3. Average-atom (AA) methods. In the specific Average-Atom model that we use, the N -nuclei

* Email address: chandre.dharma@yahoo.ca

problem is reduced to a one-body (i.e., one-ion) problem using an ion-ion XC functional to construct a neutral-pseudo-atom (NPA) model; this is an exact DFT procedure, to the extent that the e-e and ion-ion XC functionals are accurate.

4. Methods based on using classical potentials that include quantum effects. Here we use the Classical-Map (CMap) procedure of Dharma-wardana and Perrot to accurately map the quantum-electron system at temperature T to a classical Coulomb fluid at an appropriate temperature T_{cf} .

We present comparisons of $S_{ab}(k)$, and other relevant quantities from these methods, for the case of the UEF, and for hydrogen plasmas. The case of two competing phases of hydrogen, viz., fully and partially ionized hydrogen is studied in detail.

II. REVIEW OF THEORETICAL METHODS

We review the features of the theoretical methods enumerated above in greater detail below, partly with an eye to understanding why these methods may not be successful in exposing phase transitions. Here we note that various QMD calculations over several decades failed to reveal a phase transition in l -carbon [22] near the diamond density; it required NPA calculations and QMD-SCAN [23] calculations to bring it to light.

We use atomic units with $\hbar = m_e = |e| = 1$, while T will usually be given in energy units of eV (1 eV = 11,604K). We also define the electron- and ion- Wigner-Seitz radii $r_s = [3/(4\pi\bar{n})]^{1/3}$, $r_{ws} = [3/(4\pi\bar{\rho})]^{1/3}$, where \bar{n} is the average free-electron density in the plasma, while $\bar{\rho}$ is the average ion density. The number of free electrons per ion (experimentally measured using a Langmuir probe in low- T plasmas) is \bar{Z} , with $\bar{Z} = \bar{n}/\bar{\rho}$. The Fermi wavevector $k_F = (2\pi^2\bar{n})^{1/3}$ and the Fermi energy $E_F = k_F^2/2$ are important scales of energy and momentum for the electron subsystem. Note that the review of Bonitz et al. [5] seems to use r_s for r_{ws} , even for partially-ionized hydrogen, without distinction.

A. N -atom DFT simulations with MD evolution of ions

N -atom Density Functional Theory (DFT) uses N nuclei, located at $\vec{R}_I, I = 1, \dots, N$ and the corresponding number of electrons. usually with $N \sim 64 - 256$. The multi-centered electron density $n(\vec{r}; \vec{R}_I)$ is calculated using Kohn-Sham theory in the fixed potential of the ions treated as in a periodic (crystalline) potential. In effect, the Hohenberg-Kohn stationary condition on the one-body electron density leads to the Kohn-Sham equation for a set of non-interacting electrons at the interacting

density.

$$\frac{\delta F([n(r)]; \vec{R}_I)}{\delta n(r)} = 0 \quad (1)$$

Thus the interacting plasma is mapped into a Lorentz plasma in QMD with the ions held fixed. Only the electron many-body problem is simplified in this manner, with the ion-ion many-body problem left intact. So, the many-ion configuration \vec{R}_I is evolved to equilibrium using classical molecular-dynamics (MD) to obtain a statistical thermal average for the multi-centered one-body density. This procedure is implemented in many commercially available computational packages [24, 25], where a choice of pseudopotentials, and $T = 0$ XC-functionals are available. Currently commercially available packages do not provide finite- T functionals. However, implementations of finite- T codes and calculations (e.g., [26, 27]) have been reported for QMD, while Ref. [28] presents orbital-free DFT applications.

The many-ion problem in QMD has to be treated “head-on” via an N -atom classical simulation. The MD procedure yields the ion-ion pair distribution function (PDF), viz., $g_{ii}(r)$, and the corresponding $S_{ii}(k)$, but further computationally costly manipulations are needed to obtain the Kubo-Greenwood response functions required for the determination of the electrical and thermal conductivities σ and κ [29]. Similarly, further manipulations are needed [30] to determine $S_{ee}(k)$ that enters into XRT spectra [21, 31, 32].

The mean number of free electrons per ion, viz., the mean ionization \bar{Z} is not easily obtained from such N -atom QMD calculations, leading to several differing estimates of \bar{Z} [33, 34]. This method, variously referred to as DFT-MD, KS-MD (Kohn-Sham MD) and QMD (quantum molecular-dynamics) [10] will be referred to here as QMD due to its brevity and wider usage. QMD is an established “workhorse” although it has several major limitations:

1. its accuracy decisively depends on the electronic exchange-correlation (XC) functional. Thus, estimates of the conductivities (σ, κ) using QMD may differ by a factor of two depending on the selected XC-functional [14].
2. Given an exact XC-functional, the Hohenberg-Kohn-Mermin theorem of DFT promises to give the total free energy F (or the ground-state energy E at $T = 0$) and the one-body distributions $n(r), \rho(r)$ of the electrons and ions. But the theory does not provide valid excitation energies or electron eigenfunctions. The Kohn-Sham method maps the interacting many-electron system to a non-interacting system and provides the one-electron energies and eigenfunctions of that *fictitious* electron system. However, they are still a good approximation in many cases; but the bands gaps etc., of the non-interacting electron system obtained by the Kohn-Sham method need further corrections if they are to represent the actual physical system. For instance, DFT calculations of solid Ge and many other semiconductors

return a metallic solid with no band gap or greatly reduced bandgaps [39, 40].

Most implementations of the Kohn-Sham method do not correct the Kohn-Sham states for self-interaction effects [35, 36], or for the discontinuities in the XC-functional across band gaps [37]. Thus, when the Kohn-Sham eigenstates and eigenfunctions are directly used for, say, the calculation of the mean ionization \bar{Z} , results with varying degrees of inaccuracy may be obtained [34, 36, 38]. These effects may be substantially corrected if the DFT-MD calculation is augmented with a GW-quasiparticle calculation [40, 41] but the computational costs becomes prohibitive, especially for finite- T applications.

3. N -atom DFT coupled with MD (i.e., QMD), with $N \sim 100 - 500$ at finite- T is computationally extremely expensive even without GW-quasiparticle corrections because the basis sets needed for the finite- T calculations increase rapidly for finite T . For instance, the recent analysis of XRTS spectra of highly compressed Be [17–19] using QMD would take months of computation, and hence many laboratories choose to remain outside such warm-dense matter studies.

Accurate orbital-free DFT methods have been a long-sought goal for speeding up these N -atom DFT calculations. However, while considerable progress has been made in developing kinetic-energy functionals [42], their accuracies remain well below Kohn-Sham calculations; they also do not provide any one-electron functions that are convenient intermediaries in calculating many physical properties of WDM systems.

4. The structure factors $S_{ab}(k)$ are available only for $k > k_0$ where k_0 depends inversely on the linear dimension of the simulation box. For instance, Moldabekov et al. [30] do not report data for $k < 1.15 \text{ \AA}^{-1}$ in their DFT-MD studies of hydrogen at 0.33 g/cc. The issue of obtaining the small- k limit of structure data is discussed further in Sec. II E.

B. Path-integral and Monte-Carlo methods

A quasi-exact method for quantum simulations is afforded by path-integral Monte Carlo (PIMC) simulations, if not for errors arising from the Fermion-Sign Problem (FSP) that increase rapidly as T/E_F decreases. [43–46]. Bonitz et al. [5] state that “When considering hydrogen at temperatures well below the electronic - degeneracy temperature, ..., fermionic PIMC (FPIMC) becomes highly inefficient because of the FSP”. Approximate methods for dealing with the FSA have been developed, and applications to WDM studies, e.g., [47, 48] and for the calculation of finite- T XC-functionals [49, 50] are well known. We refer to all these approximate methods as PIMC for brevity.

We use in this study the PIMC results at $r_s = 2$, and 3.32 for warm dense hydrogen provided by Moldabekov et al. [30] to compare with similar results from an approach

based on a classical-map of the quantum electron system where a statistically equivalent classical Coulomb gas is studied.

C. Limitations of PIMC and QMD

Given that both PIMC and N -atom DFT-MD (i.e., QMD) are computationally very demanding, and may take months of calculation for analyzing current state-of-the-art experiments, accurate first-principles methods that are also computationally very efficient are badly needed. These methods do not yield emergent properties of complex systems, e.g., H-atoms, or excitons as the description is only in terms of electrons and nuclei. Capability for fast prediction would enable the experimentalist to optimize the diagnostics and settings “on-the-fly”, i.e., while the experiment is in progress. For instance, we may consider the prediction of the XRT spectra, or, at the more fundamental level, the prediction of pair-potentials $V_{ii}(r)$, structure factors $S_{ee}(k)$ within computational times of a few seconds as an objective for theory development.

D. Average-atom models

A serious bottleneck in N -atom DFT is the need to calculate Kohn-Sham states for tens of thousands of ionic configurations in resolving the ion-ion many-body problem, when this can actually be reduced to a *single* Kohn-Sham calculation. That is, the ion-ion many-body problem can also be rigorously reduced to a one-body problem in DFT using an appropriate ion-ion XC functional [51], just as the electron-electron problem is reduced to an effective one-electron problem using an e-e XC functional. In effect, instead of using just Eq. 1 dealing with only electrons, we consider two coupled equations. The first of these is for the electron subsystem with the one-body density $n(r)$, and the second deals with the ion one-body density $\rho(r)$. We are considering a uniform system with the mean electron density \bar{n} and a mean ion density $\bar{\rho}$. The resulting analysis leads to the construction of a single representative atom of a single nucleus placed in the appropriate plasma medium. It is referred to here as the neutral-pseudo-atom (NPA) model [51]. It is a rigorous DFT model where e-e and ion-ion many body effects are reduced to suitable one-body XC-functionals, while certain electron-ion correlations [52] have been neglected. The latter was the main criticism leveled by Chihara [53] against the NPA model of Dharma-wardana and Perrot [51]. Details of computationally convenient implementations of the NPA have been given in many past publications [13, 54, 55].

While the NPA begins as an all electron calculation, it constructs, internally, many intermediate quantities to simplify the calculation and enlighten the physical picture. These involve defining an average ionization \bar{Z} ,

ion-electron pseudopotentials, T-matrices, as well as ion-ion pair potentials and pair distribution functions. All intermediate quantities other than XC functionals are directly computed from the results of the Kohn-Sham calculations. So, given the material density $\bar{\rho}$, the nuclear charge Z_n , and the temperature T , the only quantities needed in the NPA from an external theory are the XC-potentials.

In the NPA, \bar{Z} is evaluated from the finite- T Friedel sum rule, using the phase shifts of the continuum electrons (see the Appendix). These continuum states are not significantly subject to self-interaction errors or XC-discontinuities. The phase shifts are calculated from the behaviour of the scattered wavefunctions in the asymptotic region, i.e., where interactions are negligible, and when the fictitious Kohn-Sham states and the physical (Dyson) states [41] asymptotically agree.

Also, the evaluation of the phase shifts is made at the minimum of the total free energy $F([n], [\rho])$ for variations in the one-body densities n, ρ . This means \bar{Z} corresponds to a full Saha-type calculation inclusive of all the many-body corrections automatically included via XC-functionals. This “automatic” free-energy minimization picture that arises in an NPA calculation is presented in some detail in Ref. [13].

That is, the NPA does not attempt to impose Yukawa or Debye-Hückel models, Lenard-Jones models, bond-order models etc., taken from outside. However, the ion-electron pseudopotentials obtained from the NPA can be *post facto* further re-parametrized for convenience and transferability, e.g., as modified Heine-Abarankov pseudopotentials [56]. The ion-ion pair-potentials can be represented by Yukawa forms augmented by a Friedel-type oscillatory tail [57]. The neglect of these oscillatory tails prevents the correct prediction of subtle liquid-liquid phase transitions, or, for instance, Martensitic-type transitions found in many materials.

It has been claimed that the NPA, or average-atom models cannot correctly simulate systems such as liquid carbon at low temperatures due to the existence of complex covalent bonds in them [58, 59]. We have demonstrated in previous publications that the ion-ion PDFs of complex fluids of materials such as C, Si, obtained using N -atom DFT-MD can also be obtained using the NPA, in close agreement with the QMD results, even close to the melting line. Since the NPA is based on static DFT, the calculated PDFs, $S_{ab}(k)$ are long-time averages where transient bonding effects demonstrated in N -Atom DFT simulations, e.g., in Ref. [58] are of no consequence to thermodynamic and static quantities such as the PDFs of uniform fluids.

E. Accessing the small- k limit

An advantage of average-atoms models such as the NPA over PIMC and QMD is that the structure factors $S_{ab}(k)$ are available for the whole range of k values includ-

ing the $k \rightarrow 0$. For instance, a QMD calculation using 64 atoms corresponds to a linear dimension of only 4 atoms, i.e., only a single nearest-neighbour to any “central” atom is treated, and the accessible k is limited to values larger than π/L . Furthermore, moving an atom in the simulation causes a density fluctuation of the order of $1/N$ and may washout any distinction between metastable states. Similarly, Rayleigh-weight calculations of XRT spectra require results at low scattering wavevectors where many-body effects become more prominent; but such calculations for small- k are extremely expensive using PIMC, QMC or QMD.

This problem of predicting small- k limits of structure data cannot be side-stepped by using “machine-learned” pair potentials (MLPs), unless the MLPs have been trained on expensive PIMC, QMC and QMD data that contain information on the small- k region. If the theoretical data were supplemented with empirical data, then the results are not *ab initio*. Furthermore, while there exists a theorem that validates the search for an universal XC-potential as a functional of the density, there is no “existence theorem” that asserts that MLPs of a general nature exist. The short-comings of such MLPs (which are usually multi-centered functions dependent on many parameters with little or no physical meaning), have been discussed recently, together with comparisons from NPA pair-potentials [57, 60, 61]. The simple NPA approach will remain very competitive even if such MLP-schemes could be widely implemented.

Furthermore, the classical-map approach discussed in Sec. V provides an inexpensive way of extending PIMC structure data to the small- k region. This is illustrated by our Cmap calculations for recovering the $S_{ee}(k)$ reported by Molabekov et al for $r_s = 2$, $T = 12.5$ eV.

F. Short-comings of the NPA model

A theoretical critique of the NPA model has been given by Chihara [53]. However, applications of the NPA to actual WDM calculations show that Chihara’s main objection (that a third XC functional to cover e-i exchange-correlation effects is lacking in the NPA) has no practical impact.

In our experience, the main short-comings of the currently implemented NPA code are as follows.

1. It is limited to uniform systems, or to well-defined crystalline systems. For instance, while the current NPA code could reproduce the high-density branch of the Ganesh-Widom pressure curve [62] for l -Si at its melting point, the low-density metastable supercooled-Si branch could not be demonstrated [20, 63].
2. The current NPA code assumes a sufficient presence of free electrons to justify the use of certain linearizations, e.g., in constructing pseudopotentials or pair potentials used within the code.
3. As it is a DFT code, the NPA eigenfunctions, eigenvalues, and level occupations are for the fictitious non-

interacting Kohn-Sham electrons. The code does not implement self-interaction corrections or the discontinuity in the XC-functional when the number of electrons changes by an integral number [37].

4. The many-body hamiltonian is rigorously replaced by a system consisting of a uniform electron gas containing embedded “hydrogen atoms” of effective charge \bar{Z} carrying a core of bound electron. NPA being a DFT theory, more complex associations like $(\text{H}_2)^+$ etc., being many-body effects, are not explicitly sorted out although their effects are included via XC-functionals. This may be viewed as a short-coming in some sense, while being a computational advantage of the theory! 5. The finite- T XC-functional implemented in the NPA code is that of Perrot and Dharma-wardana (PDW-XC) [64], based on the classical-map hyper-netted-chain model. This is usually not a practical limitation as structure factors, free energies, EOS etc., calculated using PDW-XC or the finite- T GDS-XC by Groth et al. [50] give very close results for typical WDM-test cases. This is established in Sec. V for the hydrogen WDMs studied here.

6. A spin-density functional treatment is not available in the current NPA code, making it unsuitable for applications to transition-metal systems at low- T .

G. The classical-map approach to WDM calculations

Attempts to use classical “statistical” potentials that mimic quantum effects has a long history [65]. The classical-map (Cmap) approach developed by the present author and Perrot [66] was motivated entirely by DFT ideas.

We noted that a fully non-local ion-ion XC-functional that is needed to reduce the ion-ion many-body problem could be internally generated within the calculation itself, using classical statistical mechanics. This means, given an accurate mapping of quantum electrons into a statistically equivalent classical Coulomb fluid, then the fully non-local XC-functionals needed for reducing the electron many-body problem could also be generated. Furthermore, the whole calculation reduces to classical statistical mechanics, avoiding the heavier machinery of quantum-statistical mechanics.

The current state of the classical map (CMap) approach is that it is quite successful in dealing with the normal uniform electron fluid (UEF) at zero to finite T , at any electron density \bar{n} and spin polarization ζ . The method can be justified using DFT. Briefly, what has been established [64, 66–73] is that the PDFs of a classical fluid (consisting of classical electrons interacting via a Coulomb-like interaction) become equal to that of the quantum UEF at the given \bar{n} , T , ζ , if the temperature T_{cf} of the classical fluid is chosen such that the XC-energy of the classical Coulomb fluid is equal to the XC-energy of the quantum fluid at the corresponding \bar{n} , T , and ζ .

At the time when the classical-map approach was de-

veloped, finite- T F_{xc} data for the UEF were not available. Hence the classical-fluid temperature T_{cf} at $T = 0$ was evaluated using the $T = 0$ XC-energy. This was named T_q , and the classical-fluid temperature T_{cf} at finite- T was estimated using the ansatz

$$T_{cf} = \sqrt{[T_q^2 + T^2]} \quad (2)$$

Here T_q depends only on the r_s of the electron fluid. Denoting the spin states as ‘ u, d ’, the classical Coulomb fluid at T_q recovers the PDFs $g_{uu}(r)$, $g_{ud}(r)$, and $g_{dd}(r)$ at $T = 0$ and for arbitrary spin polarizations ζ . Here we are concerned with the case $\zeta = 0$, and more details of CMap calculations may be found in Refs. [66, 70, 73].

In effect, since there is no Hartree contribution in uniform fluids, the total free energy is simply the XC-energy. DFT asserts that when two systems modeled to have the same Hamiltonian have the same free energy, then their one-body distributions, viz., $n(r) = \bar{n}g_{ee}(r)$ become equivalent. That is, the $g_{ee}(r)$ of the classical fluid becomes equivalent to that of the quantum fluid.

While the classical map is successful for mapping the quantum UEF, it is of limited success with partially ionized hydrogen plasmas [70–73], or for more complex systems like aluminum plasmas. Even in the fully ionized case, while the effective classical temperatures for the e-e and i-i interactions are evidently T_{cf} and T , the temperature T_{ei} of the electron-ion interaction is open to modeling. Such a temperature can be constructed via the compressibility sum rule [70], or by demanding that $g_{ei}(r)$ be consistent with that of an NPA calculation. However, as with PIMC calculations, for sufficiently high T , the CMap method can be used. That is, at high T , the differences among T , T_{cf} , or T_{ei} become small and the method begins to work well.

In this study we present CMap calculations of $S_{ab}(k)$ for fully ionized hydrogen for comparison with PIMC calculations where available. Such comparison are a necessary step for improving the classical-map approach and other computationally fast methods.

III. THE DEGREE OF IONIZATION \bar{Z} FOR WARM DENSE HYDROGEN

Although a system of N protons interacting with N electrons via the Coulomb potential seems a clear problem in quantum statistical mechanics, it turns out to be very complex, given the possibility of bound states of electrons and ions, phase transitions etc. Initially, prior to first-principles methods, various phase-transitions involving normal electronic states and even superconducting states had been conjectured [74, 75]. Today, we have rigorous tools for studying partially or fully ionized hydrogen plasmas. However, even the very concept of “the degree of ionization” [76] has been challenged, leading to insightful discussions of the topic [77, 78].

Bonitz et al. [5] state that: “the degree of ionization and the fractions of atoms and

molecules are not physical observables. They cannot be rigorously computed, even by a first principles simulation. Any result depends on the used criterion, . . . , even though the sensitivity to the chosen criterion can be verified and minimized”.

More specifically, such computations cannot even distinguish and differentiate the physical species H, H⁻, (H₂)⁺, etc., that are formed through bound-electron effects that manifest in partially ionized plasmas. The computed $g_{\text{HH}}(r)$, i.e., the proton-proton PDF $g_{\text{pp}}(r)$, obtained from such methods, for such partially ionized plasmas may contain a featureless broad peak, or usually an extra “hump” prior to the main peak, with no species differentiation.

Other authors have also claimed that there is “no quantum operator” corresponding to the “degree of ionization” in disputing the use of \bar{Z} in WDM calculations [79–81]. They use the temperature T although it too has no quantum operator in quantum mechanics. In the study of WDM, we use quantum *statistical* mechanics, with a classical heat bath attached to the system rather than a purely quantum mechanical system. Hence, quantities such as the temperature T , the chemical potential μ , and the mean ionization \bar{Z} can be introduced as Lagrange multipliers of the theory [51]. They can also be introduced into numerical simulations by introducing thermostats (for T), numberstats (for μ), as well as chargestats (for \bar{Z}). While the use of thermostats is well developed, the other types of controls for the number of particles or charge neutrality have not been taken up extensively. This is partly why quantities like \bar{Z} remain currently unacknowledged in first-principles simulations.

Furthermore, as discussed in Ref. [19] and in the Appendix, a quantum operator whose mean value gives us a precise value of \bar{Z} via the Friedel sumrule can be constructed. The mean charge \bar{Z} arises naturally within the neutral-pseudo-atom model of DFT. There is no difficulty in unambiguously defining \bar{Z} for a strict Lorentz plasma with no e-e and i-i interactions. The one-electron states and their occupations are hydrogenic and provide the same \bar{Z} either from the occupation numbers or from the Friedel sumrule. When interactions are present, there are no one-electron states, as they become Dyson quasiparticle states [41] and naive definitions of \bar{Z} fail. DFT switches off the e-e and i-i interactions by constructing fictitious Kohn-Sham states (of a modified Lorentz plasma) that provide the total density and the total free energy correctly.

The PIMC method uses Feynman trajectories but do not attempt to distinguish what may be termed bound and free electrons paths at any stage of its calculation. In effect *it has set up no machinery* to identify and distinguish species like H, (H₂)⁺, H₂, H⁻ that exist in a partially ionized H-plasma. That does not mean that these species have no “physical existence” but it shows the need to extend PIMC to capture more complex “emergent” statistical quantities. In fact, a broadened unre-

solved “bump” appears in the $g_{\text{HH}}(r)$ calculated by current PIMC methods.

In reality, the PIMC, QMD or NPA calculations, all of which begin with an input of electrons and nuclei, should be regarded as a sequence of successive calculations that can be used to analyze the speciation in hydrogen and other partially ionized plasmas in an appropriate manner, as the primary plasma, i.e., electrons and nuclei, respond to changes in different energy and length scales. New structures appear as new poles of the S -matrix (expressed in terms of particle trajectories), and in appropriate response functions that can in principle be calculated within PIMC., if these emergent entities are to be made manifest.

Even at the static level, PIMC and QMC methods can calculate $S_{ee}(k)$ as well as $S_{ii}(k)$. Experimentally, while $S_{ii}(k)$ can be obtained from X-ray or neutron diffraction, $S_{ee}(k)$ is obtained from XRTS measurements. Then, the compressibility sumrule and charge neutrality together lead to the following relations, enabling an unambiguous experimental or theoretical estimate of \bar{Z} .

$$S_{NN}(k) = S_{ee}(k) + S_{ii}(k) + 2S_{ei}(k) \quad (3)$$

$$S_{NN}(k \rightarrow 0) = (\bar{\rho} + \bar{n})T\xi \quad (4)$$

$$S_{ee}(k \rightarrow 0) = 2\bar{Z}S_{ei}(k \rightarrow 0) - \bar{Z}^2S_{ii}(k \rightarrow 0) \quad (5)$$

The equation 5 follows from the charge-neutrality requirement that $\bar{n} = \bar{Z}\bar{\rho}$ and that the total charge-charge structure factor reduces to zero as $k \rightarrow 0$. Furthermore, When $\bar{n}g_{ei}(r)$ is identified with the free-electron charge at an ion, these relations can be further simplified to give direct access to \bar{Z} . The free-electron pile-up around an in the NPA is such that:

$$n_f(r) = \Delta n_f(r) + \bar{n} = \bar{n}g_{ei}(r) \quad (6)$$

$$S_{ei}(k=0) = \int [g_{ei}(r) - 1] 4\pi r^2 dr \quad (7)$$

$$\bar{Z} = S_{ee}(k \rightarrow 0)/S_{ii}(k \rightarrow 0). \quad (8)$$

In Eq. 4, ξ is the isothermal compressibility of the system of electrons and ions. The recovery of these $k \rightarrow 0$ limits of $S_{ab}(k)$ in a simulation or via a physical model like the NPA establishes the thermodynamic consistency of the calculation since ξ is directly obtained from the EOS. In fact, the MHNC equation uses this relation to check its treatment of bridge-diagram contributions to the potential of mean force in classical-fluid theory [82].

PIMC and QMC, being limited by the simulation box size, cannot cheaply access the $k \rightarrow 0$ limit of any of the structure factors; but this is not an existential objection against \bar{Z} . The compressibility sumrule given above is not used in NPA calculations to determine \bar{Z} because $S_{ee}(k)$ is not directly available from an NPA calculation.

IV. METASTABLE STATES AND PLASMA-PHASE TRANSITIONS IN HYDROGEN

Another much-discussed feature of partially ionized plasmas is the possible existence of metastable states within regions of liquid-liquid (plasma-plasma) phase transitions [13, 20, 21, 23, 83–86]. Bonitz et al. [5], in their review of hydrogen conclude that there is still no hard evidence for a plasma-phase transition (PPT) in spite of many claims for it. Many papers that propose a PPT use intuitive physical models. Margo et al., [86] used PIMC-methods and proposed in 1996 a PPT at ~ 1 eV and $r_s \sim 2.2$. This has not been confirmed by subsequent studies. However, Filinov et al. [87, 88] used PIMC methods, simulating 50 electrons and 50 ions, and found that at $T \sim 10\,000$ K, in the density range of 0.1 g/cc...1.5 g/cc, strong density fluctuations and the formation of metallic clusters (i.e., presumably regions predominantly with $\bar{Z} = 1$) occurred, but without clear convergence of the simulations. Here we study the 0.1 g/cc isochore and provide comprehensive evidence for two competing plasma states, using DFT methods.

Some of proposed PPTs involve changes in short-ranged order [89]. Other PPTs may not show significant changes in short-ranged order as reflected in the PDFs. Instead, they involve the cooperative action of a large numbers of atoms and distant neighbours in the tails (large- r) of PDFs. Such transitions, (e.g., Martensitic transitions) are beyond the reach of simulations that employ a few hundred nuclei. Formation of such metastable phases may occur without any change in \bar{Z} [20, 21, 23], or they may have two different average ionizations at a given density and temperature. In the latter case, \bar{Z} becomes a quick label for indicating such phases. For instance, hydrogen at a given density and temperature may exist as a fully ionized metastable phase with $\bar{Z} = 1$, or with a value less than unity. Whether they “co-exist” with phase separation, or with the formation of spinodal phases etc., are topics beyond the scope of the present study.

Moldabekov et al. [30] have studied hydrogen at $T = 4.8$ eV and density 0.08 g/cc ($r_{ws} = 3.23$). Hydrogen plasmas within that range of densities are typical of those that have been proposed (see Fig. 4 of the review by Bonitz et al., [5]) to have PPTs due to competing metastable states, with $\bar{Z} = 1$ or $\bar{Z} < 1$. In Fig. 1 we display the behaviour of \bar{Z} for a hydrogen plasma of density 0.10 g/cc ($r_{ws} = 3$) over a wide range of temperatures to illustrate the competition between a fully ionized phase and a partially ionized phase. The region indicated by a box, within the temperature region 2 eV to 6 eV is characterized by two possible plasma phases that we could reach by starting our NPA calculations from either (a) a fully ionized trial solution or (b) from a partially ionized initial starting point. This behaviour is found in a variety of H-plasmas for $r_{ws} \sim 3$, possibly including the plasma with $\bar{\rho} = 0.08$ g/cc studied in Ref.[30] using PIMC.

In Fig. 2, we display the proton-proton PDF, viz.,

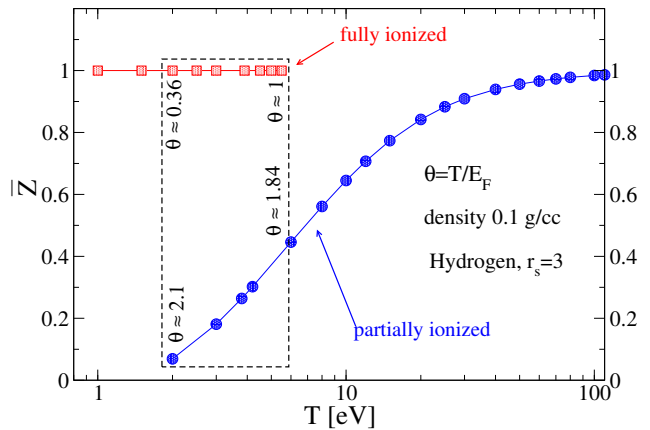


FIG. 1. (online color) The competition and possible co-existence of a partially ionized phase with $\bar{Z} < 1$, with a fully ionized phase with $\bar{Z} = 1$ for the hydrogen isochore. $\bar{\rho} = 0.1$

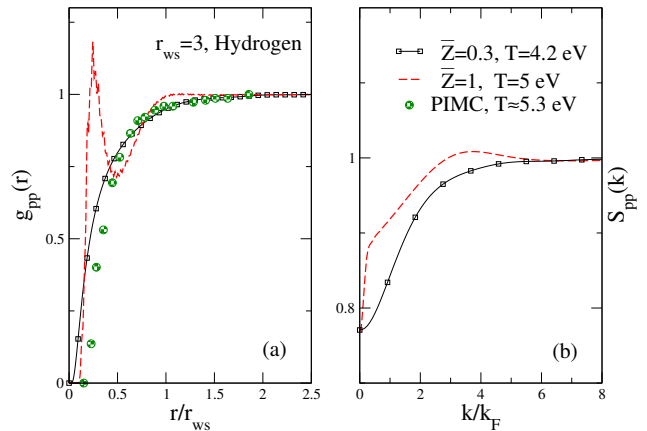


FIG. 2. (online color) The proton-proton pair distribution function $g_{pp}(r)$ and the corresponding $S_{pp}(k)$ for a fully-ionized plasma ($\bar{Z} = 1$), and for a partially ionized plasma ($\bar{Z} = 0.3$) from within the metastable region, for the density $\bar{\rho} = 0.1$ g/cc, i.e., $r_{ws} \simeq 3$. The PIMC $g(r)$ is from Ref. [5], Fig. 18, where the conditions $r_s = 3$, $T = 62500$ K are specified, with \bar{Z} unspecified.

$g_{pp}(r)$ in panel (a), and the corresponding structure factor $S_{pp}(k)$ in panel (b) for two H-plasmas of density 0.1 g/cc. We also display the closest available (in terms of density and temperature) restricted PIMC simulation of $g(r)$, extracted from Fig. 18 of Bonitz et al. [5]. The $g(r)$ with a sharp peak is on the fully-ionized branch, while the other is on the partially ionized branch. The “physical reason” for the existence of these two possibilities becomes clear from their PDFs.

The $g(r)$ of the fully-ionized system has a sharp peak near $r = 0.75$ atomic units, and also a broad peak near $r = 3$ atomic units. The convergence in this region is difficult. Although the ion-ion potential is repulsive, by placing a nearest-neighbour proton at $r < 1$ a.u., the system prevents the formation of bound electrons in atomic

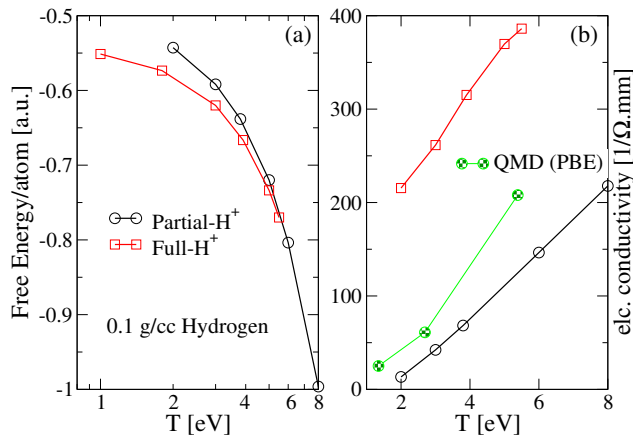


FIG. 3. (online color) (a) The Helmholtz free energy F per atom (Hartrees) for the partially-ionized plasma (labeled partial- H^+), compared with the fully ionized plasma (labeled full- H^+). (b) The electrical conductivities of the partially-ionized and fully-ionized plasmas, both of density 0.1 g/cc are displayed, calculated using a T-matrix approach suitable for strong scattering. The QMD values of σ are from the calculation by Holst et al. [91] using the $T = 0$ PBE-XC functional.

or molecular states; but it gains stability by increased XC-energy, in holding a high free-electron density, with the plasma remaining in the fully ionized state at $r_s = 3$ and $r_{ws} = 3$. The alternative possibility is to allow atomic and quasi-molecular forms of hydrogen to form, gaining stability by reducing the ion-ion electrostatic repulsion, while sacrificing the XC-energy when the free-electron density decreases, with r_s dropping from 3 to 4.48 while r_{ws} remains 3.

To obtain a converged PDF on the partially ionized branch at 5 eV itself proved difficult. However, the results at $T = 4.2$ eV, $\bar{Z} = 0.3$ are presented (curve marked with squares as data points) as being typical of this regime. Here, although $r_{ws} = 3$, r_s is 4.48 as 70% of the electrons are in bound states. The interactions among the bound forms (quasi-molecules) are weak, and hence the $g_{pp}(r)$ is seen to be rather featureless, although screening is also weak at $r_s = 4.48$. As we could not find a PIMC or QMD calculation at the temperatures of interest, we display the case $T \sim 5.3$ for which PIMC calculations are displayed in Fig.18 of Ref. [5]. While the PIMC $g(r)$ falls on the partially-ionized branch for larger r , there is disagreement in the small- r region. The origin of this difference is not clear at present.

The competition between the two hydrogen phases, namely, full- H^+ and partial- H^+ , is best quantified by comparing their Helmholtz free energies per atom. In panel (a) of fig. 3 we display the Helmholtz Free energy $F(r_{ws}, r_s, \theta)$ calculated as in Eq. 9. We have omitted the ideal classical gas free energy in the plot as it is the same for both phases.

$$F(r_{ws}, r_s, \theta) = F_{\text{uef}}(r_s, \theta) + F_{\text{emb}}(r_{ws}, r_s, \theta) + F_{12} + F_{\text{ideal}} \quad (9)$$

The first term in F is the contribution from the UEF contained in each phase. This depends on \bar{Z} which determines r_s . The second term, F_{emb} is the energy of embedding a proton in the electron fluid. This process involves (i) the creation of a bound core of electrons, (ii) a modification of the continuum density of states which are occupied by the electron-charge pileup Δn_f of Eq. 6, and (iii) setting up the particle-density profiles $n(r)$, $\rho(r)$ around the nucleus, creating pseudo-ions of charge \bar{Z} . The term $F_{12}(r_{ws}, r_s, \theta)$ represents the contributions from ion-ion interactions. The details of how these terms could be calculated relatively straight-forwardly are given in Refs. [13, 54].

The comparison of the Helmholtz free energies of the two phases shows that there is a region within $T = 4$ to 6 eV where the free energies of the two phases become comparable. Furthermore, \bar{Z} plays the role of a miscibility parameter in this competing system of two phases. When we consider a partially ionized H-plasma, e.g., at $T = 4.2$ eV with $\bar{Z} = 0.302$, it implies that the various charge-neutral species of hydrogen found in the partially ionized plasma will tolerate a mixing of ionized components (e.g., H^+ , $(H_2)^+$ etc.) up to about $\sim 30\%$. Since \bar{Z} has been calculated by a minimization of the Helmholtz free energy (via the energy-minimum principle associated with DFT), any increase or decrease in \bar{Z} (by dissolving or precipitating protons) is energetically unfavorable and triggers phase separation.

Given the total free energy, all other EOS quantities can be evaluated. In Fig. 4 we display the pressure for the fully- and partially- ionized states along the 0.1 g/cc isochore. We also display the sum of the kinetic pressure p_0 and the finite- T XC-pressure p_{xc} as P_{uef} for the two cases. It is seen that P_{uef} is a significant component of the total pressure, especially for the fully-ionized phase. The classical ideal gas pressure is the same for both phases, and is included in P_{tot} although the corresponding F_{ideal} was not included in the free-energy plot. PIMC calculations for the pressure at 0.1 g/cc are available from Militzer et al., [90], and from Table VII and Fig.14 of Ref. [5]. Since these authors do not calculate a value for \bar{Z} , they refer to the density of the system using $r_s = 3$, whereas we specify the system with $r_{ws} = 3$, while the value of r_s depends on $\bar{Z}(T)$. Our calculated pressures (along the two metastable branches) are very close to each other within numerical uncertainties. The pressure of the partially ionized branch, which is the only one that survives for $T > 6$ eV agrees closely with the PIMC pressure data.

Fig. 3(b) displays the electrical conductivity σ of the partially-ionized phase, compared with the fully ionized phase, calculated using finite- T XC, i.e., PDW-XC, and a T-matrix to include strong scattering. The fully ionized phase has a high conductivity. The QMD calculations of σ by Holst et al., [91] use a $T = 0$ PBE-XC functional. QMD does not distinguish two possible plasma phases. Given the well-known sensitivity of QMD- σ to the XC-functional, the agreement is satisfactory.

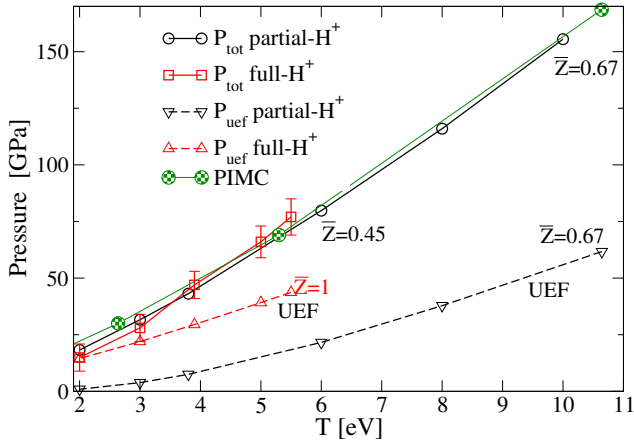


FIG. 4. (online color) The total pressures along the 0.1 g/cc isochores of the two phases, calculated from the Helmholtz free energy F are displayed. The UEF contributions are also displayed. The PIMC data are from Militzer et al. [90].

The picture of the hydrogen plasma used in our calculations is that of many pseudo-ions of charge \bar{Z} (carrying their ionic- and electronic- screening envelopes) interacting with one another. If we consider the plasma at $T = 6$ eV, $\bar{\rho} = 0.1$ g/cc, these pseudo-ions have a charge of 0.446. However, this does not mean that *in reality*, there are such pseudo-ions of charge 0.446 in the plasma at any instant. What it means is that the long-time thermodynamic average of various types of ions and neutrals that exist in the plasma can be represented as a statistically averaged object with a charge of 0.446. Such a statistical model gives a pressure (and other properties such as X-ray structure data) in very close agreement with that from PIMC where the averaging is carried over particle trajectories. One may ask if a proper book-keeping of electron trajectories may perhaps be used to construct these pseudo-ions from the trajectories to recover the DFT one-body picture.

Since the DFT used in the NPA reduces the many-body problem to effective non-interacting one body objects (electrons, pseudo-ions), it does not construct have objects like $(\text{H}_2)^+$ although their effect on the densities and free energies are fully accounted for. In contrast, the PIMC has not made such a reduction of the many-body problem and it should, in principle, be able to develop methods of identifying complex multi-center objects such as $(\text{H}_2)^+$, H_2 et cetera.

V. CLASSICAL MAP CALCULATIONS FOR THE UEF AND H-PLASMAS

Although the classical-map (Cmap) method is not as well grounded as the NPA method for general WDMs, the CMap works well for fully ionized plasmas. Furthermore, it provides a very accurate treatment of the UEF and was used to construct a sophisticated e-e XC

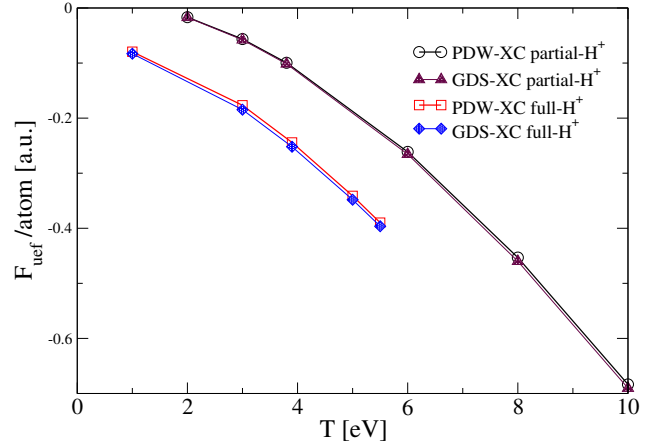


FIG. 5. (online color) The UEF components of the total Helmholtz free energy F per atom (Hartrees) for the partially-ionized plasma (labeled partial- H^+), and for the fully ionized plasma (labeled fully- H^+) at 0.1 g/cc, calculated using the classical map (i.e., PDW-XC) [64], and via the parametrization given by Groth et al. (GDS-XC) [50] are displayed.

functional [66] prior to the advent of QMC and PIMC-based XC functionals. The method has been successfully applied to calculating XC-energies and pair-distribution functions of reduced dimensional systems that arise in the physics of nano-structures [67, 69, 92–94]. In fact, since the current NPA code uses the finite- T PDW-XC functional, here we establish that it is adequate for the calculations presented here, using comparisons with the functional of Groth et al. [50].

A major contribution to the Helmholtz free energy F given in Eq. 9 is the UEF component $F_{\text{uef}}(r_s, \theta)$. We calculate F_{uef} using the PDW-XC fit used in the NPA, as well as with the fit formula for F_{uef} given by Groth et al. (GDS-XC) for the two phases, partial- H^+ and full- H^+ . The results are presented in Fig. 5, and cover a regime of r_s and T such that $1 < r_s < 8$, and $1 \text{ eV} < T < 10 \text{ eV}$. As the stabilization of the fully-ionized H^+ plasma against the partially-ionized plasma is largely controlled by the free energy of the UEF, the good agreement between F_{uef} calculated in the NPA using PDW-XC, with that of GDS-XC shows (i) that the Cmap provides a reliable XC functional for these WDM calculations, and (ii) that the identification of two competing plasma states reported here is not likely to be modified by the use of alternative e-e XC-functionals.

The Cmap for the UEF requires only the electron parameter r_s , the spin polarization ζ and the physical temperature as inputs. The spin polarization will be taken as zero, as WDM studies have currently addressed mainly the case $\zeta = 0$. However, the capacity to do spin-polarized calculations is important since many giant planets and other astrophysical objects have strong magnetic fields.

A. Calculations using the Classical Map for the UEF

The importance of the e-e structure factor $S_{ee}(k)$ has been emphasized in recent work [30]. We also noted the relevance of $S_{ee}(k \rightarrow 0)$ in regard to the concept of \bar{Z} (see Eq. 8) and the compressibility sumrule .

There have been many calculations of the structure factors $S_{e,e}(k, \zeta)$ and PDFs of the uniform electron fluid at $T = 0$, using mainly fixed-node Monte Carlo, and diffusion Monte-Carlo methods. Comparisons of results from the CMap for $T = 0$, both for $\zeta = 0$ and $\zeta \neq 0$, were given in previous publications [66]. In this study we limit ourselves to more recent finite- T UEF calculations. In this context we select the following densities \bar{n} and temperatures T , as PIMC H-plasma calculations are also available for most of them. We use $\theta = T/E_F$ in the following.

1. $r_s = 2$, i.e., nominally $\bar{n} = 0.33$ g/cc at $T = 4.8$ eV. In Ref. [30], $\theta = 1, 0.5$, and 0.25 are equated with $T = 12.5$ eV, 6.27 eV and 3.13 eV. This is consistent with an assumed ionization of $\bar{Z} = 1$ in hydrogen. NPA calculations at $r_s = 2, T = 12.5$ eV, 6.25 eV, and 3.13 eV confirmed that they can be treated as fully ionized plasmas with $\bar{Z} = 1$. No co-existence or competition of partially ionized states was encountered.

However, Ref. [30] also uses a ‘chemical model’ with $\bar{Z} = 0.72, 0.64$, and 0.61 . The case $\bar{Z} = 0.72$ should correspond to $\theta = 1.26, r_s = 2.247$, while $\bar{Z} = 0.64$ implies $\theta = 0.683, r_s = 2.337$; and $\bar{Z} = 0.51$ implies that $\theta = 0.352, r_s = 2.375$. The authors have not indicated how these \bar{Z} values have been obtained. We do not examine these cases any further in this study.

In the case the UEF, we do not concern ourselves with \bar{Z} , and we simply use $r_s = 2, \theta = 1, 0.5$ and 0.25 for comparisons with the results given in the literature. In the case of H-plasmas, a first-principles determination of \bar{Z} becomes necessary. Ref. [30] has not reported PIMC calculations for $\theta = 0.5, 0.25$ as PIMC is not viable at low temperatures. They have provided results based on a *new ansatz* combining time-dependent DFT results for the dynamic structure factor $S_{ee}(q, \omega)$ with static DFT results for the density response.

2. $r_s = 3.23$, i.e., nominally $\bar{n} = 0.08$ g/cc at $T/E_F = 1$, and given as 4.8 eV in Ref. [30] imply a value of $\bar{Z} = 1$. Furthermore, Ref. [30] refers to a ‘chemical model’ (CM), where a mean ionization of $\bar{Z} = 0.57$ is used. If $\bar{Z} = 1$ were assumed, then setting $\theta = 1$ is consistent. However, the value of \bar{Z} for this hydrogen plasma (i.e., 0.08 g/cc at 4.8 eV), obtained using the Friedel sum rule implemented via the NPA code gives $\bar{Z} = 0.365$, significantly lower than the chemical models used by Moldabekov et al. [30]. If the NPA value of \bar{Z} is adopted then, $r_s = 4.519$, while $\theta = 1.956$. Hence we are unable to make a proper comparison with the results given in Fig. 1 of the study by Moldabekov et al [30].

However, as seen from Fig. 1 for hydrogen at 0.1 g/cc, a density of 0.08 g/cc at 4.8 eV is a good candidate for being in a fully ionized state *and also* in a partially ion-

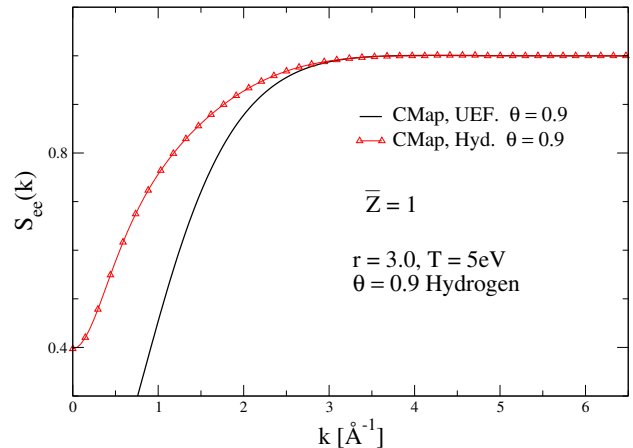


FIG. 6. (online color) The e-e structure factor $S_{ee}(k)$ at $r_s = 3, \theta = 0.897$ for the uniform electron fluid (UEF), and for fully ionized hydrogen calculated using the Classical Map (CMap) method.

ized state. Unfortunately, even on starting with fully ionized trial inputs, we could not generate Kohn-Sham NPA solutions at 0.08 g/cc and 4.8 eV that were fully ionized. As a somewhat close approximation to the density (0.08 g/cc) studied by Moldabekov et al., in Fig. 6 we display the $S_{ee}(k)$ for fully ionized hydrogen, and the corresponding UEF, at $r_s = 3, \bar{\rho} = 0.1$ g/cc and at 5.0 eV.

VI. CLASSICAL MAP AND NPA CALCULATIONS FOR H-PLASMAS

Moldabekov et al. [30] provide PIMC calculations for $S_{ee}(k)$ for hydrogen plasmas at the density 0.33 g/cc, and at $\theta = 1, 0.5$ and 0.25 . We have used the nomenclature ‘uniform electron fluid’ (UEF) for quantum electron systems with a uniform non-responding neutralizing positive background. The name ‘uniform electron gas’ is also used by many authors, most appropriately if $r_s < 1$. As already noted, it has been shown [66] with good accuracy that the quantum electron fluid at a physical temperature T is statistically equivalent to a classical Coulomb fluid at the temperature T_{cf} , Eq. 2. Now that results for $F_{xc}(T)$ for the UEF are readily available, the ansatz used in Eq. 2 is not necessary and T_{cf} can indeed be calculated directly, but choosing T_{cf} to recover the known $F_{xc}(r_s, T)$ from a classical-fluid calculation. However, in this study we retain the original ansatz whose accuracy was checked in Fig. 5.

VII. CONCLUSION

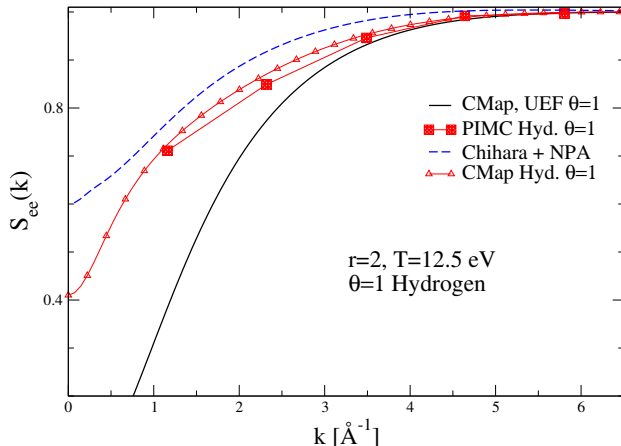


FIG. 7. (online color) The e-e structure factor $S_{ee}(k)$ at $r_s = 2$, $\theta = 1$ for the uniform electron fluid (UEF), and for fully ionized hydrogen. Solid black line is $S_{ee}(UEF, k)$ for the UEF calculated using the CMap approach. The corresponding result for fully ionized hydrogen (red line with triangles) is to be compared with the PIMC results (filled red squares) reproduced from Ref. [30]. The dashed blue line is $S_{ee}(k)$ constructed according to Chihara’s prescription, with the relevant quantities calculated using the NPA method.

A. Results for $r_s = 2$, $\theta = 1$

Figure 7 is essentially similar to Fig. 4 of Ref. [30], and treats the case $\theta = 1$, $\bar{\rho} = 0.33$ g/cc, at 12.5 eV which corresponds to $r_s = 2$ since the system is fully ionized.

An approximate form of S_{ee} proposed by Chihara [95] can also be calculated using the so-called “ion feature” $I(k)$ of XRTS theory, using the bound electron-density $n_b(k)$ and the screening density $n_f(k)$ that is formed around each ion of nuclear charge Z_n . In the present case there are no bound electrons, with $\bar{Z} = 1$ and $n_b(k) = 0$.

$$I(k) = \{n_b(k) + n_f(k)\}^2 S_{ii}(k) \quad (10)$$

$$S_{ee}(k) = S_{ee}(UEF, k) + I(k)/Z_n \quad (11)$$

Chihara’s approximation does not satisfy the compressibility sumrule for a two component fluid unless the compressibility of the UEF is negligible. We have calculated the relevant quantities, viz., $n_f(k)$, $S_{ii}(k)$ using the NPA and constructed S_{ee} according to Eq. 10. This is displayed (dashed blue line) in Fig. 7. We find that the Chihara approach is only moderately successful here, unlike with more dense plasmas, e.g., highly compressed Be studied in Ref. [19]. In contrast, the results of the CMap approach seem to be in agreement. Furthermore, the Cmap, if applicable, provides an inexpensive approach to extending the limited structure data from PIMC and QMD towards the $k \rightarrow 0$ limit.

Our study of hydrogen plasmas presented here has demonstrated the existence of competing states of ionization in partially ionized hydrogen plasmas in the liquid state. For instance, for $r_{ws} \sim 3$ and for temperatures such that $0.35 < T/E_F \leq 1$, two competing energy and length scales arise wherein a high-density electron fluid stabilized by its XC-energy competes with a partially ionized plasma with a high embedding energy. The mean ionization \bar{Z} is also interpreted to be a measure of the degree of miscibility of the fully ionized H-phase in the completely un-ionized (covalent-like) H-phase.

We used a first-principles method, namely, one-atom density functional theory where both the e-e and ion-ion many-body problems have been reduced to one-body problems. This one-body DFT approach, computationally realized as the NPA model, uses two XC-functionals (one for electrons, and another for ions), where the e-e functional is taken in as an external input.

We have also used a classical-map scheme where the electron subsystem is replaced by a statistically equivalent classical Coulomb-type fluid whose temperature is selected to reproduce the correlation energy of the quantum fluid at $T = 0$. The exchange energy is exactly treated by the selection of the non-interacting PDFs of the finite- T UEF. This classical-map approach allows a convenient, numerically very fast treatment of fully ionized hydrogen (at higher temperatures), whereby all the structure factors (including the electron-electron structure factor) can be computed.

The further characterization of competing metastable states of ionization in partially ionized H-plasmas (as revealed in this study) is important, both from the point of view of basic physics, as well as in regard to applications in astrophysics and high-energy density physics. Furthermore, the development of theoretical tools to expose and identify the atomic and quasi-molecular species (such as H, H_2^- , H_2 , H^- etc.) that exist in partially ionized plasmas, but not revealed by current PIMC and QMC calculations, is also an important task for future research.

Appendix A

1. The finite- T Friedel sumrule and \bar{Z}

Unlike ion-ion scattering which is largely repulsive, electron-ion scattering is attractive and close interactions and multiple scattering effects are important. The continuum wavefunctions are asymptotically like phase-shifted plane waves. Denoting the radial part of the free-electron-like Kohn-Sham functions of energy $\epsilon_k = k^2/2$ by $R_{kl}(r)$, we have the asymptotic form:

$$R_{kl}(r)|_{r \rightarrow \infty} \simeq \sin[kr - l\pi/2 + \delta_l(k)]/kr \quad (A1)$$

where $\delta_l(k)$ is the phase shift. The phase shift is related to the scattering operator $\hat{S}_l(k)$ of the S -matrix by the relation [96]:

$$\hat{S}_l(k) = \exp\{2i\tilde{\delta}_l(k)\} \quad (\text{A2})$$

The phase shift is a number, an observable that connects the incoming wave with the outgoing wave. The scattering operator acting on the incoming wave transforms it to the phase shifted outgoing wave.

Keeping in mind that $\delta_l(k)$ is an observable directly related to the scattering operator, we may define, for convenience, a phase-shift operator $\hat{\delta}_l(k)$ such that its meanvalue is the c -number $\delta_l(k)$. We may also define a thermal and quantum averaging of an operator via:

$$\langle \hat{g}(\epsilon) \rangle = \int_0^\infty d\epsilon \left\{ -\frac{df(\epsilon)}{d\epsilon} \right\} \langle \hat{g}(\epsilon) \rangle \quad (\text{A3})$$

We consider the sum over the continuum states averaged over the thermal distribution. The Friedel sumrule asserts that this sum is equal to the charge of the scattering center, identified as \bar{Z} . The $T = 0$ form was given by Friedel in 1952 [97], while the finite- T version was given in 1982 in Ref. [51].

$$\bar{Z} = \frac{2}{\pi T} \int_0^\infty k f(\epsilon_k) \{1 - f(\epsilon_k)\} \quad (\text{A4})$$

$$\times \sum_l (2l+1) \delta_l(k) dk \quad (\text{A5})$$

$$f(\epsilon_k) = 1 / [1 + \exp\{(k^2/2 - \mu^0)/T\}]. \quad (\text{A6})$$

In the NPA, as we are dealing with non-interacting (Kohn-Sham) electrons, the non-interacting chemical potential μ^0 and the unmodified density of states is used at this stage. Furthermore, we have given a scattering-operator type formulation as some authors have claimed that there is “no quantum operator” corresponding to \bar{Z} . The above average is in fact a quantum *statistical* average involving the thermal distribution as well.

The phase shifts are used for calculating the value of \bar{Z} in each iteration of the NPA equations until consistency is obtained. The phase shifts are also used to calculate the modified density of continuum states that is used in evaluating the embedding free energy appearing in Eq. 9, and in the T-matrix evaluation of the conductivity.

2. The Kohn-Sham energy levels and phase shifts of the NPA at $T = 10$ eV, 0.1 g/cc

As an example of the Kohn-Sham structure of a neutral-pseudo-atom for hydrogen, we consider the case of $T = 10$ eV, $\bar{\rho} = 0.1$ g/cc. In this case, the Friedel sum gives $\bar{Z} = 0.645$.

Only one bound-electron energy level, viz., $1s$ exists

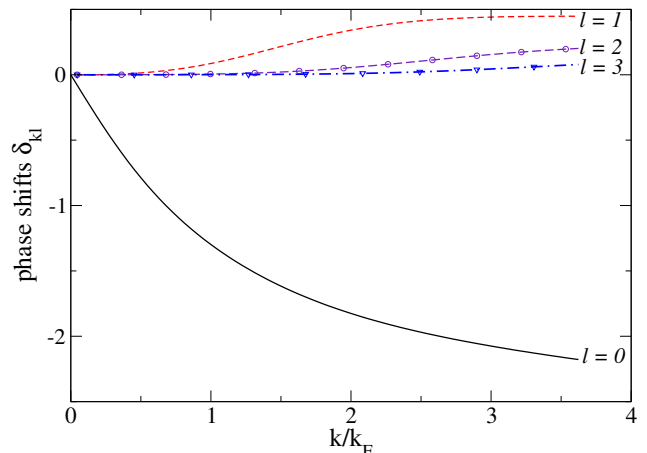


FIG. 8. (online color) The phase shifts of the $l = 0, 1, 2, 3$ angular momentum states of the free-electron wavefunctions of the neutral pseudo-atom of a hydrogen plasma for the case of $T = 10$ eV and density 0.1 g/cc.

The Kohn-Sham states $|n, l, \epsilon\rangle, |k, l, \epsilon\rangle$ are a complete set that describes electronic states in the field of a proton *and* its accompanying density distributions $\rho(r), n(r)$, that together with the pseudoatom. This means, even the effects of $(\text{H}_2)^+$ and more complex arrangement of protons and electrons consistent with $\rho(r)$ are contained in the electron distribution $n(r)$ predicted by the above (complete set of) Kohn-Sham states. The observables $\rho(r), n(r)$ and \bar{Z} are static averages. The $1s$ energy level and its energy shift (compared to that in atomic hydrogen) are that of a fictitious electron and need not agree with spectroscopic measurements.

Phase shifts of angular momentum states from 0 to 3 are presented as a function of k in Fig. 8. They become negligible for high energy states and high angular momentum states. A sufficient number of k, l states are used in the numerical work, and even higher-energy contributions are treated by Thomas-Fermi theory. These details are given in Ref. [13, 54].

[1] P. B. Corkum, *Attosecond science* Nature physics **3** 381 (2007).

[2] D. Kremp, T. Bonarth, M. Bonitz and M. Schlanges.

Phys. Rev. E **60**, 4725 (1999).

[3] A. Ng, T. Ao, F. Perrot, M.W.C. Dharma-wardana, M.E. Ford, *Laser and particle beams*, **23**, 527-537 (2005).

- [4] M. Bonitz, *Quantum Kinetic Theory*, Springer (2016).
- [5] Michael Bonitz, Jan Vorberger, Mandy Bethkenhagen, Maximilian P. Böhme, David M. Ceperley, Alexey Filinov, Thomas Gawne, Frank Graziani, Gianluca Gregori, Paul Hamann, Stephanie B. Hansen, Markus Holzmann, S. X. Hu, Hanno Khelet, Valentin V. Karasiev, Uwe Kleinschmidt, Linda Kordts, Christopher Makait, Burkhard Militzer, Zhandos A. Moldabekov, Carlo Pierleoni, Martin Preising, Kushal Ramakrishna, Ronald Redmer, Sebastian Schwalbe, Pontus Svensson, Tobias Dornheim/m. *Physics of Plasmas* **31**, 110501 (2024).
- [6] A. Filinov and M. Bonitz, *Phys. Rev. E* **108**, 055212 (2023).
- [7] H Poole, M. K. Ginnane, M. Millot, H. M. Bellenbaum, G. W. Collins, S. X. Hu, D. Polsin, R. Saha, J. Topp-Mugglestone, T. G. White, D. A. Chapman, J. R. Rygg, S. P. Regan, and G. Gregori. *Physical Review Research* **6**, 023144 (2024). DOI: 10.1103/PhysRevResearch.6.023144
- [8] R.P. Drake, *High-Energy-Density Physics: Foundation of Inertial Fusion and Experimental Astrophysics*, Graduate Texts in Physics (Springer International Publishing, 2018).
- [9] R. Betti, O. A. Hurricane, *Inertial-confinement fusion with lasers*, *Nature Physics* **12**, 435-448 (2016).
- [10] J.A. Gaffney, Suxing Hu, P. Arnault..E. Zurek et al. *High Energy Density Physics*, Aug 2018 <https://doi.org/10.1016/j.hedp.2018.08.00>
- [11] E. E. McBride, A. Krygier, A. Ehnes, E. Galtier, M. Harmand, Z. Konôpková, H. J. Lee, H.-P. Liermann, B. Nagler, A. Pelka, M. Rödel, A. Schropp, R. F. Smith, C. Spindloe, D. Swift, F. Tavella, S. Toleikis, T. Tschentscher, J. S. Wark and A. Higginbotham. *Nature Phys.* **15**, 89-94 (2019).
- [12] L. Harbour, G. D. Förster, M. W. C. Dharma-wardana, and Laurent J. Lewis. *Phys. Rev. E* **97**, 043210 (2018).
- [13] F. Perrot and M.W.C. Dharma-wardana, *Phys. Rev. E.* **52**, 5352 (1995).
- [14] L. J. Stanek, A. Kononov, S. B. Hansen, et al. *Phys. Plasmas*, **31**, 052104 (2024).
- [15] G. Gregori, S. H. Glenzer, W. Rozmus, R. W. Lee, and O. L. Landen. *Phys. Rev. E* **67**, 026412 (2003).
- [16] S. H. Glenzer and Ronald Redmer, *Rev. Mod. Phys.* **81**, 1625 (2009).
- [17] T. Döppner, M. Bethkenhagen, D. Kraus, P. Neumayer, D. A. Chapman, B. Bachmann, R. A. Baggott, M. P. Böhme, L. Divol, R. W. Falcone, L. B. Fletcher, O. L. Landen, M. J. MacDonald, A. M. Saunders, M. Schörner, P. A. Sterne, J. Vorberger, B. B. L. Witte, A. Yi, R. Redmer, S. H. Glenzer, and D. O. Gericke. *Nature* **618**, 270-275 (2023).
- [18] T. Dornheim, H. M. Bellenbaum, M. Bethkenhagen, S. B. Hansen, M. P. Böhme, T. Döppner, L. B. Fletcher, Th. Gawne, D. O. Gericke, S. Hamel, D. Kraus, M. J. MacDonald, Zh. A. Moldabekov, Th. R. Preston, R. Redmer, M. Schörner, S. Schwalbe, P. Talias, and J. Vorberger. *Phys. Plasmas* **32**, 052712 (2025).
- [19] M. W. C. Dharma-wardana and D. D Klug, *Phys. Rev. E* **111**, 065208 (2025).
- [20] M.W.C. Dharma-wardana, Dennis D. Klug, and Richard C. Remsing *Phys. Rev. Lett.* **125**, 075702 (2020). doi: 10.1103/PhysRevLett.125.075702
- [21] M. W. C. Dharma-wardana, D. D. Klug, Hannah. Poole, and G. Gregori. *Phys. Rev. E* **111**(1) 015205 (2025).
- [22] Hull, C. J., Raj, S. L., &. Saykally, R. J. *Chemical Physics Letters* **749**, 137341 (2020).
- [23] M. W. C. Dharma-wardana and Dennis D. Klug, *Phys. Plasmas* **29**, 022108 (2022); doi: 10.1063/5.0077343
- [24] G. Kresse and J. Furthmüller, *Phys. Rev. B* **54**, 11169 (1996). <https://www.vasp.at>
- [25] X. Gonze, B. Amadon, G. Antonius, F. Arnardi, et. al. *Computer Physics Communications* **248**, 107042. (2020). <https://doi.org/10.1016/j.cpc.2019.107042>.
- [26] V. V. Karasiev, S. X. Hu, M. Zaghoo, and T. R. Boehly, ?Exchange-correlation thermal effects in shocked deuterium: Softening the principal hugoniot and thermo-physical properties. *Phys. Rev. B* **99**, 214110 (2019).
- [27] K. Ramakrishna, T.Dornheim, and Jan Vorberger. *Phys. Rev. B* **101**, 195129 (2020); Erratum, **112**, 119901 (2025).
- [28] V. V. Karasiev, T. Sjoström, S. B. Trickey, *Computer Physics Communications*, **185** 2340-3249 (2014).
- [29] V. Recoules and J. P. Crocombette, *Phys. Rev. B* **72**, 104202 (2005).
- [30] Zhandos A. Moldabekov, Xuecheng Shao, Hannah M. Bellenbaum, Cheng Ma, Wenhui Mi, Sebastian Schwalbe, Jan Vorberger, and Tobias Dornheim. arXiv:2507.00688v1 [physics.plasma-ph] (2025).
- [31] K-U Plageman, H. R. Rüter, T. Bornath, Mohammed Shihab, Michael P. Desjarlais, C. Fortmann, S. Glenzer, R. Redmer. *Phys. Rev. E* **92**, 013103 (2015).
- [32] L. Harbour, M. W. C. Dharma-wardana, D. Klug and L. Lewis. *Physical Review E* **94**, 053211, (2016).
- [33] P.A. Sterne S.B. Hansen, B.G. Wilson, W.A. Isaacs, *High Energy Density Phys.* **3**, 278 (2007).
- [34] Mandy Bethkenhagen, Bastian B. L. Witte, Maximilian Schörner, Gerd Röpke, Tilo Döppner, Dominik Kraus, Siegfried H. Glenzer, Philip A. Sterne, and Ronald Redmer. *Phys. Rev. Research* **2**, 023260 (2020).
- [35] J. P. Perdew and Alex Zunger *Phys. Rev. B* **23**, 5048 (1981).
- [36] M.W.C. Dharma-wardana, Ionization of carbon at 10-100 times the diamond density and in the 10⁶ K temperature range. *Phys. Rev. E* **104**, 015201 (2021).
- [37] W. Kohn *Phys. Rev. B* **33**, 4331(R) (1986).
- [38] Faussurier, G., Blancard, C. & Bethkenhagen, M. *Phys. Rev. E* **104**, 025209 (2021).
- [39] L. J. Sham and Schlüter, *Phys. Rev. B* **32**, 3883 (1985). Density functional theory of the bandgap.
- [40] M. A. Hybertson and S. G. Louie, *Phys. Rev. Lett.*, **55**, 1418 (1985).
- [41] F. Perrot and M. W. C. Dharma-wardana, *Phys. Rev. A* **29**, 1378 (1984).
- [42] W. Mi, K. Luo, S. B. Trickey, M. Pavonello, *Chemical Reviews*, **123**, 12039 (2023).
- [43] E. Y. Loh, J. E. Gubernatis, R. T. Scalettar, S. R. White, D. J. Scalapino, and R. L. Sugar. *Phys. Rev. B* **41**, 9301?9307 (1990).
- [44] M. Troyer and U. J. Wiese, *Phys. Rev. Lett.* **94**,170201 (2005).
- [45] T. Dornheim, *Phys. Rev. E* **100**, 023307 (2019).
- [46] T. Dornheim, T. Döppner, P. Talias, M. P. Böhme, L.B. Fletcher, Th. Gawne, F. R. Graziani, D. Kraus, M. J. MacDonald, Zh. A. Moldabekov, S. Schwalbe, D.O. Gericke, and J. Vorberger. arXiv:2402.19113v1 [physics.plasmas-ph] (2024).
- [47] K. P. Driver, B. Militzer, *Phys. Rev. Lett.* **108**, 115502 (2012).
- [48] Shuai Zhang, Burkhard Militzer, Lorin X. Benedict,

- François Soubiran, Philip A. Sterne, and Kevin P. Driver *J. Chem. Phys.*, **148** (10), 102318 (2018).
- [49] Ethan W. Brown, J. L. Dubois, J. L. Dubois, Markus Holzmann, David Ceperley *Phys. Rev. B* **88**, 081102(R) (2013).
- [50] S. Groth, T. Dornheim, T. Sjostrom, F.D. Malone, W. Foulkes, M. Bonitz, *Phys. Rev. Lett.* **119** (13) 135001 (2017). <http://dx.doi.org/10.1103/PhysRevLett.119.135001>.
- [51] M. W. C. Dharma-wardana and F. Perrot. *Phys. Rev. A* **26**, 2096 (1982).
- [52] F. Perrot, Y. Furutani and M.W.C. Dharma-wardana, *Phys. Rev. A* **41**, 1096-1104 (1990).
- [53] J. Chihara, *Phys. Rev. A* **41**, 1247 (1991).
- [54] F. Perrot, *Phys. Rev. E* **47**, 570 (1993).
- [55] M. W. C. Dharma-wardana, Proceedings of the Conference on Density Functional Theory, Debrecen, 2015. Edited by K. Schwarz and A. Nagy. *Computation* **4** (2), 16; (2016).
- [56] M. W. C. Dharma-wardana, and François Perrot, *Phys. Rev. E* **58**, 3705 (1998).
- [57] M. W. C. Dharma-wardana, Lucas J. Stanek, and Michael S. Murillo *Phys. Rev. E* **106**, 065208 (2022).
- [58] S. Hamel, Lorin X. Benedict, Peter M. Celliers, M. A. Barrios, T. R. Boehly, G. W. Collins, Tilo Döppner, J. H. Eggert, D. R. Farley, D. G. Hicks, J. L. Kline, A. Lazicki, S. LePape, A. J. Mackinnon, J. D. Moody, H. F. Robey, Eric Schwegler, and Philip A. Sterne, *Phys. Rev. B* **86**, 094113 (2012).
- [59] H. D. Whitley, D. M. Sanchez, S. Hamel, A. A. Correa, and L. X. Benedict, *Contrib. Plasma Phys.* **55**, 390 (2015).
- [60] Lucas J. Stanek, Raymond C. Clay III, M. W. C. Dharma-wardana, Mitchell A. Wood, Kristian R. C. Beckwith, and Michael S. Murillo, *Phys. Plasmas* **28**, 032706 (2021).
- [61] M. W. C. Dharma-wardana, *Physics of Plasmas* **28**, 052108 (2021); <https://doi.org/10.1063/5.0047642> Simple pair-potentials and pseudo-potentials for warm-dense matter and general applications.
- [62] P. Ganesh, and M. Widom, *Phys. Rev. Lett.* **102**, 075701 (2009).
- [63] Richard C. Remsing and Michael L. Klein, *J. Phys. Chem* 2020 <https://dx.doi.org/10.1021/acs.jpcc.0c01798>
- [64] F. Perrot and M. W. C. Dharma-wardana, *Phys. Rev. B* **62**, 16536 (2000); *Erratum:* **67**, 79901 (2003); arXiv-1602.04734.
- [65] A. V. Filinov, V. O. Golubnychiy, M. Bonitz, W. Ebeling, and J. W. Dufty. *Phys. Rev. E* **70**, 046411 (2004).
- [66] M. W. C. Dharma-wardana and F. Perrot, *Phys. Rev. Lett.* **84**, 959 (2000).
- [67] François Perrot and M. W. C. Dharma-wardana, *Phys. Rev. Lett.* **87**, 206404 (2001).
- [68] Dufty, J.; and Dutta, Sandipan; *Phys. Rev. E.* **87**, 032101 (2013).
- [69] M. W. C. Dharma-wardana, D. Neilson and F. M. Peeters *Phys. Rev. B* **99**, 035303 (2019).
- [70] R. Bredow, Th. Bornath, W.-D. Kraeft, M.W.C. Dharma-wardana and R. Redmer *Contributions to Plasma Physics*, **55**, 222-229 (2015). DOI 10.1002/ctpp.201400080
- [71] M. W. C. Dharma-wardana, *Phys. Rev. B* **100**, 155143 (2019). DOI: 10.1103/PhysRevB.100.155143
- [72] Yu Liu and Jianzhong Wu, *J. Chem. Phys* **141** 064115 (2014).
- [73] Dharma-wardana, M. W. C.; and Perrot, F.; *Phys. Rev. B* **66**, 014110 (2002).
- [74] G. E. Norman, A. N. Starostin, *High Temp.* **6**, 394 (1968).
- [75] N. W. Ashcroft, Metallic hydrogen: A high-temperature superconductor? *Phys. Rev. Lett.* **21**, 1748-1749 (1968).
- [76] M. S. Murillo, J. Weisheit, S. B. Hansen, and M. W. C. Dharma-wardana, *Phys. Rev. E* **87**, 063113 (2013).
- [77] Thomas Gawne, Sam M. Vinko, and Justin S. Wark. *Phys. Rev. E* **103**, L023201 (2024).
- [78] V. Sharma and A. J. White, *Phys. Rev. Lett.* **134**, 095102 (2025).
- [79] R. Piron and T. Blenski, *Phys. Rev. E* **83**, 026403 (2011).
- [80] S. X. Hu, L. A. Collins, V. N. Goncharov, J. D. Kress, R. L. McCrory, S. Skupsky. *Physics of Plasmas*, **23**, 042704 (2016).
- [81] Nadine Wette and J-C Pain, *Phys. Rev. E* **108**, 015205 (2023).
- [82] F. Lado, S. M. Foiles and N. W. Ashcroft, *Phys. Rev. A* **26**, 2374 (1983).
- [83] W. Ebeling, and W. Richert. *Physics Letters A*, **108** 80 (1985).
- [84] D. Saumon, and G. Chabrier. *Phys. Rev. Lett.* **62**, 2397 (1989).
- [85] (1992). S. T. Weir, A. C. Mitchell, and W. J. Nellis, Metallization of fluid molecular hydrogen at 140 GPa (1.4 Mbar), *Phys. Rev. Lett.* **76**, 1860-1863 (1996).
- [86] W. R. Magro, D. M. Ceperley, C. Pierleoni, and B. Bernu, Molecular dissociation in hot, dense hydrogen, *Phys. Rev. Lett.* **76**, 1240-1243 (1996).
- [87] V. Filinov, V. Fortov, M. Bonitz, and P. Levashov, Phase transition in strongly degenerate hydrogen plasma, *Jetp. Lett.* **74**, 384 (2001).
- [88] V. Filinov, M. Bonitz, P. Levashov, V. Fortov, W. Ebeling, and M. Schlanges, Plasma phase transition in hydrogen and electron-hole plasmas, *Contrib. Plasma Phys.* **43**, 290-294 (2003).
- [89] G. E. Norman and I. M. Saitov. *Doklady Physics*, **62**, No. 6, pp. 284-288. (2017). Original Russian, G.E. Norman, I.M. Saitov, *Doklady Akademii Nauk*, **474** (5) 553-557 (2017).
- [90] B. Militzer, F. Gonzalez-Cataldo, S. Zhang, K. P. Driver, and F. Soubiran, *Phys. Rev. E* **103**, 013203 (2021).
- [91] B. Holst, M. French, and R. Redmer, Electronic transport coefficients from ab initio simulations and application to dense liquid hydrogen, *Phys. Rev. B* **83**, 235120 (2011).
- [92] M. W. C. Dharma-wardana and F. Perrot, *Phys. Rev. Lett.* **90**, 136601 (2003).
- [93] D. Jost and M. W. C. Dharma-wardana *Phys. Rev. B* **72**, 195315 (2005).
- [94] Chieko Totsuji, Takashi Miyake, Kenta Nakanishi, Kenji Tsuruta and Hiroo Totsuji *J. Phys.: Condens. Matter* **21** 045502 (2009).
- [95] J. Chihara, *J. Phys.: Condens. Matter* **12**, 231 (2000).
- [96] U. Fano and A. R. P. Rau, *Atomic collisions and spectra*. New York, Academic. (1986).
- [97] J. Friedel, *Philosophical Magazine*, **43**, 153 (1952).